2011 American Control Conference
on O'Farrell Street, San Francisco, CA, USA
June 29 - July 01, 2011

Multi-variable iterative tuning of a variable gain controller with application to a scanning stage system

Marcel Heertjes Tufan Tepe Henk Nijmeijer

Abstract— **Toward improved performance of fast and nano-accurate motion systems an iterative tuning procedure for the parameters of a variable gain controller is presented. Under constrained optimization, optimal values for the variable gain parameters are found by minimizing a quadratic function of the servo error signals in a representative sampled-data interval. An effective method for improved performances is demonstrated on a scanning stage system, using a combined model/data based approach in obtaining the gradients with respect to the parameters to be optimized.**

I. INTRODUCTION

In industry fast and nano-accurate tracking systems are found for example in wafer scanners for lithography [10] and storage drives in consumer electronics [8]. In an attempt to overcome linear design trade-offs, advanced nonlinear feedback is used atop a nominal linear control design [1], [7], [11]. In this context a variable gain controller whose feedback gains vary according to the occurrence of disturbances shows potential in dealing with position dependent dynamics and disturbances [3].

The variable gain controller essentially has two parameters: a gain and a switching length. The gain is constrained to assure stable closed-loop dynamics. The switching length does not influence the closed-loop stability result (hence its choice is stability invariant) and thus appears strictly performance driven. It is the aim of this paper to obtain both controller parameters automatically using an iterative tuning procedure. For a similar procedure but considering single parameter optimization, see [4] in which the switching length is optimized under less stringent stability constraints. For multi-variable switching control based on iterative feedback tuning (or IFT) see [6].

In the iterative parameter tuning scheme used in this paper, the necessary gradients with respect to the parameters to be optimized are obtained from a model/data-based approach. Using machine-in-the-loop optimizations [9], this provides the machine-specific fine tunings needed to further improve servo performances. Convergence of the scheme is shown under strict conditions [2], [5]. More specifically, in the presence of noise and uncertainty an invariant set is found to which all solutions converge. This follows from Lyapunov arguments and is confirmed by measurements.

The paper is organized as follows. In Section II the variable gain controller is discussed in the context of motion control systems. Section III introduces a lifted system representation for the nonlinear closed-loop dynamics. In Section IV an iterative parameter tuning scheme is discussed for the optimization of the variable gain and switching length. Stability is addressed in Section V using Lyapunov analysis whilst performance is assessed in Section VI by measurement on a stage system. Section VII recaps the main conclusions and recommendations of the work.

M.F. Heertjes, T. Tepe, and H. Nijmeijer are with the Department of Mechanical Engineering, Eindhoven University of Technology, 5600 MB Eindhoven, The Netherlands m.f.heertjes@tue.nl, t.tepe@student.tue.nl, h.nijmeijer@tue.nl

II. VARIABLE GAIN CONTROL

The aim in variable gain control is to have high-gain disturbance rejection properties of the closed loop while keeping a small-gain noise response. Without surpassing the Bode sensitivity integral, this is achieved by acting on the non-stationary occurrence of the disturbances through proportionally switching between high-gain and low-gain controllers. Since switching to a high-gain controller (hence inducing improved disturbance rejection properties) only occurs incidentally, the variable gain controlled system (on average) keeps a low-gain noise response.

The variable gain controller is used as add-on to a nominal linear feedforward/feedback controller structure. This is schematically shown in Fig. 1. In the nominal control

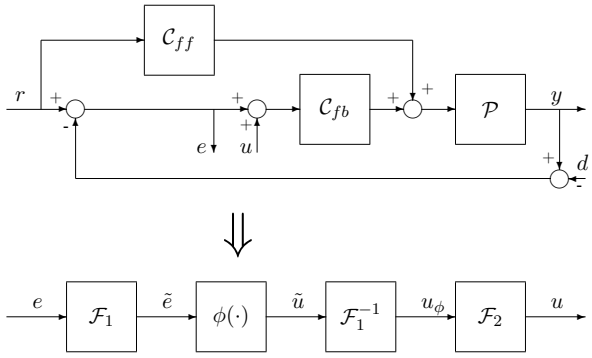

Fig. 1. Block diagram of a variable gain control system.

design (the upper part of the figure), $\mathcal{P}$ represents a single-input single-output linear time-invariant plant, $\mathcal{C}_{ff}$ represents a feed-forward controller which aims at approximating inverted plant dynamics using acceleration (second derivative) and snap (fourth derivative) contributions, and $\mathcal{C}_{fb}$ represents a single-input single-output feedback controller. Motion is dictated by the reference command r. Subtraction of the plant output y then gives the servo error signals e. Additionally $\mathcal{P}$ is subjected to disturbances d along with the output of the variable gain controller u. The latter (see the lower part of the

TABLE I

MAXIMUM GAIN VALUES FROM CIRCLE CRITERION EVALUATION

axis	x	y	z
$\mathcal{S}_c$	0.66	0.77	0.77
$\mathcal{F}_2\mathcal{S}_c$	3.60	3.84	5.38

figure) consists of a series connection of weighting filters $\mathcal{F}_1$, variable gains $\phi(\cdot)$, and loop-shaping filters $\mathcal{F}_2$; see [3] for a more detailed description regarding the design of these filters. Here it suffices to state that $\mathcal{F}_1$ is often a notch-type filter used to amplify the main disturbances to be suppressed in e. Based on the output signal $\tilde{e}$ extra suppression is induced by the variable gain $\phi(\tilde{e})$:

$$\phi(\tilde{e}) = \begin{cases} 0, \text{ if } |\tilde{e}| \leq \delta, \\ \alpha - \dfrac{\alpha\delta}{|\tilde{e}|}, \text{ otherwise,} \end{cases} \tag{1}$$

which has two parameters: the gain α and the switching length δ. The variable gain output signal $\tilde{u}$ is filtered by the inverse weighting filter operation $\mathcal{F}_1^{-1}$ as to obtain stability invariance with respect to the weighting filter design [3]. The resulting signal u_ϕ is input to a loop shaping filter $\mathcal{F}_2$ before being added to the nominal feedback loop.

The loop shaping filter $\mathcal{F}_2$ is designed to guarantee closed-loop stability of the nonlinear feedback loop using the following absolute stability argument.

Theorem 1: Consider the strictly proper plant $\mathcal{P}$ that is stabilized by $\mathcal{C}_{fb}$ under uniformly bounded disturbances r and f. The variable gain controller (in the lower part of Fig. 1) with stable and proper filters $\mathcal{F}_1$ and $\mathcal{F}_2$ renders the closed-loop system stable if

$$\Re\{\mathcal{S}_c^*(j\omega) = \mathcal{F}_2(j\omega)\mathcal{S}_c(j\omega)\} \geq -\frac{1}{\alpha}, \tag{2}$$

with the complementary sensitivity function $\mathcal{S}_c$ of the nominal controlled system defined by

$$\mathcal{S}_c(j\omega) = \mathcal{C}_{fb}(j\omega)\mathcal{P}(j\omega)\mathcal{S}(j\omega), \tag{3}$$

and the sensitivity function $\mathcal{S}$ defined by

$$\mathcal{S}(j\omega) = \frac{1}{1 + \mathcal{C}_{fb}(j\omega)\mathcal{P}(j\omega)}. \tag{4}$$

Proof: The proof stems from the circle criterion. ■

In (2) the choice for the switching length δ does not influence the stability result. The switching gain α does influence stability although its value can be constrained beforehand.

From the lithographic industry, the example of a scanning stage is adopted: a floating mass that performs a controlled meandering motion; see [4] for a system description, transfer functions, and parameter values. For this system the (measured) complementary sensitivity functions of the nominal control system $\mathcal{S}_c(j\omega)$ are depicted in the left part of Fig. 2. The scaled complementary sensitivity functions $\mathcal{S}_c^*(j\omega)$ are depicted in the right part. The maximum gains satisfying (2) are given in Table I for the x, y, and z axes. Without

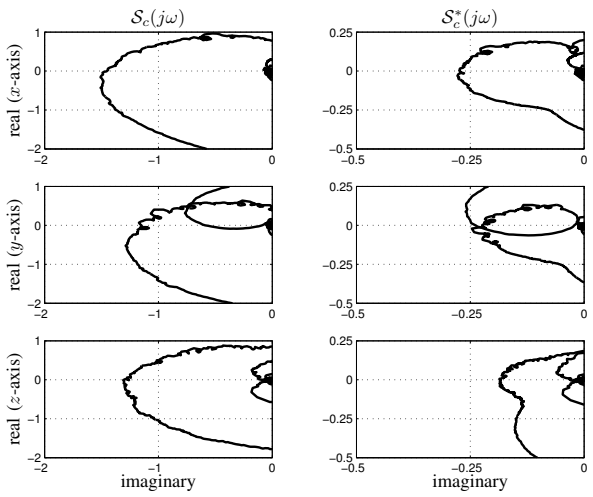

Fig. 2. Nyquist diagram of the variable gain control system used for closed-loop stability evaluation.

loop shaping filter ($\mathcal{F}_2 = 1$) extra gain values for α remain limited to 70% of the nominal gain. With the considered loop shaping filter ($\mathcal{F}_2 \neq 1$) the extra gain can be chosen 5.38 times the nominal gain (z-axis).

Having thus an upper bound on α the question arises how to tune α and δ as to achieve best servo performances. For this purpose an extremum seeking optimization approach is studied which utilizes the so-called lifted representation of the nonlinear closed-loop dynamics.

III. LIFTED SYSTEM REPRESENTATION

Consider the set of algebraic equations:

$$\begin{aligned} \mathbf{e}_k &= -\mathbf{S}_c^*\mathbf{F}_1^{-1}\tilde{\mathbf{u}}_k + \mathbf{S}\mathbf{r} + \mathbf{S}\mathbf{d}_k \\ \tilde{\mathbf{e}}_k &= \mathbf{F}_1\mathbf{e}_k \\ \tilde{\mathbf{u}}_k &= \alpha_k\varphi(\tilde{\mathbf{e}}_k), \end{aligned} \tag{5}$$

representing the stable variable gain controlled stage dynamics of Fig. 1 in lifted system description; k represents a trial (or iteration). The constant matrices $\mathbf{S}_c^*$, $\mathbf{F}_1$, and $\mathbf{S} \in \mathbb{R}^{n\times n}$ represent Toeplitz matrices (related to the previously introduced frequency response functions) of the form

$$\mathbf{T} = \begin{bmatrix} a_1 & 0 & \dots & 0 \\ a_2 & a_1 & \dots & 0 \\ \vdots & \vdots & \ddots & \vdots \\ a_n & a_{n-1} & \dots & a_1 \end{bmatrix}, \tag{6}$$

with $a_1, a_2, \dots, a_n$ Markov parameters (a_1 being the first response sample to a unitary impulse). $\mathbf{r} = [r(1) \dots r(n)]^{\mathrm{T}} \in \mathbb{R}^n$ are the trial-invariant reference commands and $\mathbf{d}_k = [d(1) \dots d(n)]^{\mathrm{T}} \in \mathbb{R}^n$ the trial varying disturbances. The error signals are given by $\mathbf{e}_k = [e(1) \dots e(n)]^{\mathrm{T}} \in \mathbb{R}^n$ and are input ($\tilde{\mathbf{e}}_k = [\tilde{e}(1) \dots \tilde{e}(n)]^{\mathrm{T}} \in \mathbb{R}^n$) to the variable gain $\varphi(\tilde{\mathbf{e}}_k) \in \mathbb{R}^n$ after being filtered by $\mathbf{F}_1$. The output $\tilde{\mathbf{u}}_k = [\tilde{u}(1) \dots \tilde{u}(n)]^{\mathrm{T}} \in \mathbb{R}^n$ is a function of the variable gain parameters α_k and δ_k. This follows from the definition

$\varphi(\tilde{\mathbf{e}}_k) = \varphi_1(\tilde{\mathbf{e}}_k)\tilde{\mathbf{e}}_k + \delta_k\varphi_2(\tilde{\mathbf{e}}_k)$ in which

$$\begin{aligned}\varphi_1(\tilde{\mathbf{e}}_k)[i,i] &= \begin{cases} 0, & \text{if } |\tilde{\mathbf{e}}_k[i]| < \delta_k, \\ 1, & \text{otherwise,} \end{cases} \\ \varphi_2(\tilde{\mathbf{e}}_k)[i] &= \begin{cases} 0, & \text{if } |\tilde{\mathbf{e}}_k[i]| < \delta_k, \\ -\text{sign}(\tilde{\mathbf{e}}_k[i]), & \text{otherwise.} \end{cases}\end{aligned} \tag{7}$$

To quantify performance of the control system underlying (5) the following objective function is considered

$$L_k = \mathbf{e}_k^{\mathrm{T}}\mathbf{e}_k, \tag{8}$$

with $\mathbf{e}_k$ the k-th time-sampled data vector in a performance interval of interest. As an example, consider stage meandering motion where full field processing is done by alternately scanning neighboring dies. To account for position-dependent dynamics and (deterministic) disturbances the to-be-optimized signal $\mathbf{e}_k$ is obtained using the concatenated error signals from five representative scans distributed along the stage, see Fig. 3. Each scan (solid,black) in y-direction is

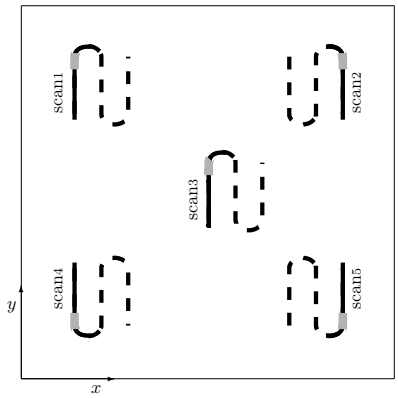

Fig. 3. Motion sets in the stage xy-plane, including pre-scans (dashed,black), scans (solid,black), and optimization intervals (solid,gray).

preceded by two pre-scans (dashed,black) as to simulate realistic motion. Representative data intervals at the beginning of each scan (solid,gray) are assigned for optimization, thus giving the performance (or optimization) interval. A proper choice for the performance interval remains application-specific and therefore difficult to generalize.

It is the aim of this paper to find the optimal set of variable gain parameters $\tilde{\mathbf{p}}$ that minimizes (8), or

$$\tilde{\mathbf{p}} := \arg\min_{\mathbf{p}_k} L_k, \tag{9}$$

with $\mathbf{p}_k = [\delta_k \ \alpha_k]^{\mathrm{T}}$. Hereto an iterative scheme is considered for machine-in-the-loop parameter optimization.

IV. ITERATIVE PARAMETER TUNING SCHEME

In finding $\tilde{\mathbf{p}}$ consider the iterative parameter tuning scheme

$$\mathbf{p}_{k+1} = \mathbf{p}_k - \beta\left(\frac{\partial \mathbf{e}_k^{\mathrm{T}}}{\partial \mathbf{p}}\frac{\partial \mathbf{e}_k}{\partial \mathbf{p}}\right)^{-1}\frac{\partial \mathbf{e}_k^{\mathrm{T}}}{\partial \mathbf{p}}\mathbf{e}_k, \tag{10}$$

with convergence rate $0 < \beta < 1$ and gradients

$$\frac{\partial \mathbf{e}_k}{\partial \mathbf{p}} = \begin{bmatrix} \dfrac{\partial \mathbf{e}_k}{\partial \delta} & \dfrac{\partial \mathbf{e}_k}{\partial \alpha} \end{bmatrix} \in \mathbb{R}^{n\times 2}, \tag{11}$$

with

$$\begin{aligned}\frac{\partial \mathbf{e}_k}{\partial \delta} &= -\alpha_k\mathbf{A}(\tilde{\mathbf{e}}_k)\varphi_2(\tilde{\mathbf{e}}_k) \in \mathbb{R}^n, \\ \frac{\partial \mathbf{e}_k}{\partial \alpha} &= -\mathbf{A}(\tilde{\mathbf{e}}_k)\varphi(\tilde{\mathbf{e}}_k) \in \mathbb{R}^n.\end{aligned} \tag{12}$$

Matrix $\mathbf{A}(\tilde{\mathbf{e}}_k) \in \mathbb{R}^{n\times n}$ is given by

$$\mathbf{A}(\tilde{\mathbf{e}}_k) = (\mathbf{I} + \alpha_k\mathbf{S}_c^*\mathbf{F}_1^{-1}\varphi_1(\tilde{\mathbf{e}}_k)\mathbf{F}_1)^{-1}\mathbf{S}_c^*\mathbf{F}_1^{-1}. \tag{13}$$

The parameter update in (10) is obtained from a model/data-based approach. In this approach, the linear complementary sensitivity $\mathbf{S}_c^*$ and the controller parts $\mathbf{F}_2$ and $\mathbf{F}_1$ in (13) are obtained from models. The nonlinear parts $\varphi_1(\tilde{\mathbf{e}}_k) \in \mathbb{R}^{n\times n}$ and $\varphi_2(\tilde{\mathbf{e}}_k) \in \mathbb{R}^n$ are constructed from data. On the one hand the (nonlinear) controller operations are exactly known and therefore can be accounted for. On the other hand plant characteristics which are not exactly known are better off being modelled and given appropriate noise filtering properties. Convergence of the scheme in (10) applied to the system in (5) is studied with Lyapunov theory.

V. LYAPUNOV STABILITY

Consider L_k in (8) to be a Lyapunov function candidate

$$L_k = \mathbf{e}_k^{\mathrm{T}}\mathbf{e}_k = \|\mathbf{e}_k\|^2, \tag{14}$$

and consider $\|\mathbf{e}_k\|_p$ the p-norm on $\mathbf{e}_k$ defined by

$$\|\mathbf{e}_k\|_p^2 = \mathbf{e}_k^{\mathrm{T}}\mathbf{P}_k\mathbf{e}_k, \tag{15}$$

with $\|\mathbf{P}_k\|^2 = \lambda_{\max}(\mathbf{P}_k^{\mathrm{T}}\mathbf{P}_k) \leq 1$ the maximum absolute eigenvalue of $\mathbf{P}_k = \mathbf{P}_k^{\mathrm{T}}$,

$$\mathbf{P}_k = \frac{\partial \mathbf{e}_k}{\partial \mathbf{p}}\left(\frac{\partial \mathbf{e}_k^{\mathrm{T}}}{\partial \mathbf{p}}\frac{\partial \mathbf{e}_k}{\partial \mathbf{p}}\right)^{-1}\frac{\partial \mathbf{e}_k^{\mathrm{T}}}{\partial \mathbf{p}}, \tag{16}$$

a positive semi-definite matrix for which holds

$$\|\mathbf{P}_k\mathbf{e}_k\|^2 = \mathbf{e}_k^{\mathrm{T}}\mathbf{P}_k^{\mathrm{T}}\mathbf{P}_k\mathbf{e}_k \leq \mathbf{e}_k^{\mathrm{T}}\mathbf{P}_k\mathbf{e}_k = \|\mathbf{e}_k\|_p^2. \tag{17}$$

From (5) (and using (12) and (13)) it follows that

$$\begin{aligned}\mathbf{e}_k &= -\mathbf{A}(\tilde{\mathbf{e}}_k)\alpha_k\delta_k\varphi_2(\tilde{\mathbf{e}}_k) + \mathbf{B}(\tilde{\mathbf{e}}_k)(\mathbf{r} + \mathbf{d}_k) \\ &= \frac{\partial \mathbf{e}_k}{\partial \mathbf{p}}\mathbf{E}^{\mathrm{T}}\mathbf{E}\mathbf{p}_k + \mathbf{B}(\tilde{\mathbf{e}}_k)(\mathbf{r} + \mathbf{d}_k),\end{aligned} \tag{18}$$

with $\mathbf{E} = [1 \ 0]$ and

$$\mathbf{B}(\tilde{\mathbf{e}}_k) = (\mathbf{I} + \alpha_k\mathbf{S}_c^*\mathbf{F}_1^{-1}\varphi_1(\tilde{\mathbf{e}}_k)\mathbf{F}_1)^{-1}\mathbf{S} \in \mathbb{R}^{n\times n}. \tag{19}$$

Similarly,

$$\mathbf{e}_{k+1} = \frac{\partial \mathbf{e}_{k+1}}{\partial \mathbf{p}}\mathbf{E}^{\mathrm{T}}\mathbf{E}\mathbf{p}_{k+1} + \mathbf{B}(\tilde{\mathbf{e}}_{k+1})(\mathbf{r} + \mathbf{d}_{k+1}). \tag{20}$$

Subtracting (18) from (20) and using (10) then leads to the following error update law

$$\mathbf{e}_{k+1} = \mathbf{e}_k - \beta\mathbf{P}_k\mathbf{e}_k + \mathcal{O}_k, \tag{21}$$

with remainder terms

$$\mathcal{O}_k = \mathbf{B}(\tilde{\mathbf{e}}_{k+1})(\mathbf{r}+\mathbf{d}_{k+1}) - \mathbf{B}(\tilde{\mathbf{e}}_k)(\mathbf{r}+\mathbf{d}_k) + \delta_{k+1}\left(\frac{\partial \mathbf{e}_{k+1}}{\partial \delta} - \frac{\partial \mathbf{e}_k}{\partial \delta}\right) - (\alpha_{k+1}-\alpha_k)\frac{\partial \mathbf{e}_k}{\partial \alpha}. \quad (22)$$

Assume these terms are bounded by uniform bound η, or $\lim_{k\to\infty} \sup \|\mathcal{O}_k\| \leq \eta$. This is reasonable since the nonlinear system in Fig.1 is bounded-input bounded-output stable within the constrained set of α. Substitution of (21) in the Lyapunov difference $L_{k+1} - L_k$ and using (22) gives

$$\begin{aligned} &L_{k+1} - L_k \\ &= (\mathbf{e}_{k+1}^{\mathrm{T}} + \mathbf{e}_k^{\mathrm{T}})(\mathbf{e}_{k+1} - \mathbf{e}_k) \\ &= -2\beta\|\mathbf{e}_k\|_p^2 + \beta^2\|\mathbf{P}_k\mathbf{e}_k\|^2 + \mathcal{O}_k^{\mathrm{T}}\mathcal{O}_k + 2\mathcal{O}_k^{\mathrm{T}}(\mathbf{I}-\beta\mathbf{P}_k)\mathbf{e}_k \\ &\leq -\beta(2-\beta)\|\mathbf{e}_k\|_p^2 + \eta^2 + 2(1+\beta)\eta\|\mathbf{P}_k\|\|\mathbf{e}_k\|. \end{aligned} \quad (23)$$

With

$$2\eta(1+\beta)\|\mathbf{P}_k\|\|\mathbf{e}_k\| \leq \zeta_k\eta^2(1+\beta)^2 + \frac{1}{\zeta_k}\|\mathbf{P}_k\|^2\|\mathbf{e}_k\|^2, \quad (24)$$

for any $\zeta_k > 0$, it follows that

$$\begin{aligned} L_{k+1} - L_k \leq \; &-\beta(1-\beta)\|\mathbf{e}_k\|_p^2 - \beta(1-\xi_k)\|\mathbf{e}_k\|_p^2 \\ &+ \eta^2(1+\zeta_k(1+\beta)^2), \end{aligned} \quad (25)$$

with

$$0 < \xi_k = \zeta_k^{-1}\beta^{-1}\frac{\|\mathbf{P}_k\|^2\|\mathbf{e}_k\|^2}{\|\mathbf{e}_k\|_p^2} < 1. \quad (26)$$

For

$$\|\mathbf{e}_k\|_p \geq \eta\sqrt{\frac{(1+\zeta(1+\beta)^2)}{\beta(1-\xi)}}, \quad (27)$$

with $\zeta = \lim_{k\to\infty}\sup\zeta_k$ and $\xi = \lim_{k\to\infty}\sup\xi_k$ satisfying (26) it therefore follows that

$$L_{k+1} - L_k \leq -\beta(1-\beta)\|\mathbf{e}_k\|_p^2. \quad (28)$$

Having a positive definite Lyapunov function candidate with a negative definite difference (provided that (27) holds) all solutions converge to an invariant set defined by (27).

Consider again the scanning stage system. Fig. 4 shows the results of dual-parameter optimization in the scanning y-direction; the switching gain α_k in the left part and the switching length δ_k in the right part. For nine sets of initial conditions resulting from three initial switching gains $\alpha_0 \in \{1.3, 2.6, 3.8\}$ and three initial switching lengths $\delta_0 \in \{0, 7, 14\}$ nm, it can be seen that convergence under fixed convergence rate $\beta = 0.3$ is obtained to an invariant set denoted by $[\overline{\alpha}_k - 3\sigma_\alpha, \overline{\alpha}_k + 3\sigma_\alpha]$ and $[\overline{\delta}_k - 3\sigma_\delta, \overline{\delta}_k + 3\sigma_\delta]$ for $k \to 40$; $\overline{\alpha}_k$ = 3.5 and $\overline{\delta}_k$ = 3.39 nm (thick dashed lines) denote the mean values and $\sigma_\alpha = 0.13$ and $\sigma_\delta = 0.33$ nm the standard deviations, respectively; the thin dotted lines denote the corresponding 3σ-values. It is clear that the variable gain controller induces best performance.

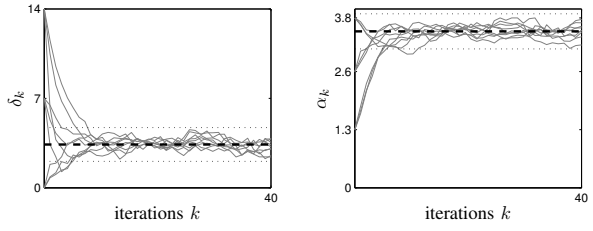

Fig. 4. Iteration diagram showing convergence of $\mathbf{p}_k = [\delta_k \; \alpha_k]^{\mathrm{T}}$ under optimization in the y-direction from nine different sets of initial conditions $\alpha_0 \in \{1.3, 2.6, 3.8\}$, $\delta_0 \in \{0, 7, 14\}$ nm; convergence rate $\beta = 0.3$; left plot: mean $\overline{\alpha}_k$ = 3.5 (thick,dashed) and $3\sigma_\alpha = 0.39$ (dotted); right plot: mean $\overline{\delta}_k$ = 3.39 nm (thick,dashed) and $3\sigma_\delta = 1.32$ nm (dotted).

The effect of the convergence rate β is depicted in Fig. 5. For three values $\beta \in \{0.1, 0.3, 1.0\}$ and one set of initial conditions with $\alpha_0 = 3.8$ and δ_0 = 0 nm, it follows that convergence improves by increasing β but with the effect of increased sensitivity to noises. As a result the invariant set to which all solutions converge tends to increase. This is clear (in particular for the switching length) by depicting the previous bounds for the mean and 3σ-values. After convergence, $\beta = 0.3$ satisfies the bounds, $\beta = 0.1$ shows slower convergence but satisfies the bounds more easily, and $\beta = 1$ shows faster convergence but violates the bounds.

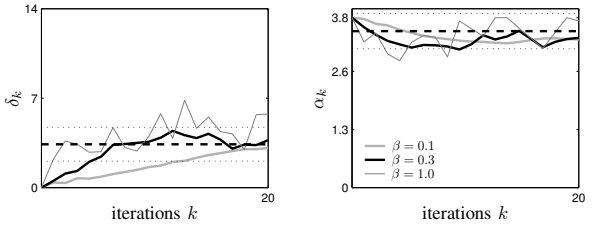

Fig. 5. Iteration diagram showing convergence of $\mathbf{p}_k = [\delta_k \; \alpha_k]^{\mathrm{T}}$ under optimization in the y-direction for three different convergence rates $\beta \in \{0.1, 0.3, 1.0\}$; $\alpha_0 = 3.8$, δ_0 = 0 nm; left plot: mean $\overline{\alpha}_k$ = 3.5 (thick,dashed) and $3\sigma_\alpha = 0.39$ (dotted) from Fig. 4; right plot: mean $\overline{\delta}_k$ = 3.39 nm (thick,dashed) and $3\sigma_\delta = 1.32$ nm (dotted) from Fig. 4.

VI. PERFORMANCE ASSESSMENT ON A SCANNING STAGE SYSTEM

To assess performance under optimized variable gain control, the scanning stage system from the previous examples is adopted. Given the optimized variable gain controller parameters, time-domain performance is shown in Fig. 6. For the y-direction, three cases are considered: the low-gain case with $\alpha_k = 0$, the high-gain case with $\alpha_k = 3.8$ and $\delta_k = 0$ nm, and the optimized case with $\alpha_k = 3.5$ and $\delta_k = 3.39$ nm. The upper part of the figure shows the corresponding time responses under scanning set-point excitation; the dashed curves show a scaled representation of the acceleration set-point. It can be seen that prior to scanning (before the zero acceleration phase) optimization induces error responses similar to the case of linear high-gain feedback. These responses are preferred over the responses associated with the case of low-gain feedback. During scanning both variable-gain and low-gain feedback induce noise responses that remain inside the switching length. Hence no additional noise amplification. This is not true for linear high-gain feedback which reveals an increased noise response.

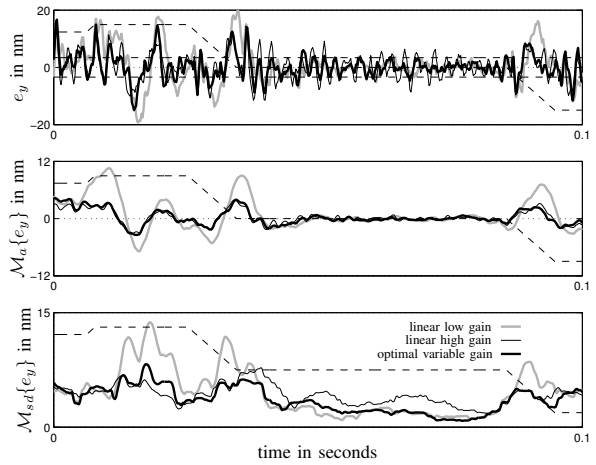

Fig. 6. Time-series measurement of the scanning performances in y-direction under optimized values $\mathbf{p}_k = [3.39\ 3.5]^{\mathrm{T}}$ either unfiltered, $\mathcal{M}_a$-filtered, or $\mathcal{M}_{sd}$-filtered; similarly the results are shown under linear low-gain control ($\mathbf{p}_k = [0\ 0]^{\mathrm{T}}$) and linear high-gain control ($\mathbf{p}_k = [0\ 3.8]^{\mathrm{T}}$); dashed curves represent the scaled acceleration set-point profile.

The above-mentioned trade-offs become more pronounced by filtering. Two filter operations are of special interest: the moving average filter operation, a low-pass filter used to quantify machine overlay:

$$\mathcal{M}_a(e_y[i]) = \frac{1}{T_p} \sum_{j=i-T_p/2}^{i+T_p/2-1} e_y[j],\ \forall i \in \{1,\ldots,n\}, \quad (29)$$

with $T_p = 44$ a process time constant expressed in an even number of time samples, and the moving standard deviation filter operation, a high-pass filter used to quantify imaging:

$$\mathcal{M}_{sd}(e_y[i]) = \sqrt{\frac{1}{T_p} \sum_{j=i-T_p/2}^{i+T_p/2-1} (e_y[j] - \mathcal{M}_a(e_y[j]))^2}. \quad (30)$$

In terms of $\mathcal{M}_a$-filtering, Fig. 6 shows that during the non-zero acceleration intervals large responses as occurring under low-gain feedback are avoided by either high-gain or optimized variable gain control. This also holds true under $\mathcal{M}_{sd}$-filtering. During scanning in the zero acceleration interval, it can be seen that low-gain feedback outperforms high-gain feedback in keeping a low-gain noise response. The optimized set of variable gain control parameters now induces a response similar to low-gain feedback and thereby combines the best of both linear control systems.

This effect also follows from the cumulative power spectral density analysis in Fig. 7. For the unfiltered time-series of Fig. 6, this figure shows that the optimized variable gain controller induces low-frequency disturbance rejection properties similar to high-gain feedback but with an improved high-frequency noise response related to low-gain feedback.

VII. DISCUSSION

Multi-variable iterative tuning of a variable gain controller gives access to improved performance which is demonstrated on a scanning stage system. The gradients needed in the parameter update law are obtained from a combined

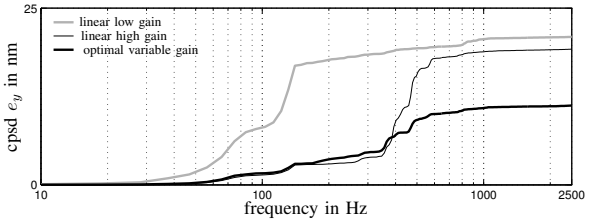

Fig. 7. Cumulative power spectral density analysis of the scanning performances in y-direction under optimized values $\mathbf{p}_k = [3.39\ 3.5]^{\mathrm{T}}$; similarly the results are shown under linear low-gain control ($\mathbf{p}_k = [0\ 0]^{\mathrm{T}}$) and linear high-gain control ($\mathbf{p}_k = [0\ 3.8]^{\mathrm{T}}$).

model/data-based approach. The data part has the advantage of controlling actual performances whereas the model part adds the necessary noise filtering. In the presence of noise and model uncertainty the solutions of the iterative parameter tuning scheme converge to an invariant set rather than an optimized value. The size of the invariant set can be reduced by lowering the convergence rate. This however comes at the price of an increased number of iterations which is undesired in practice and which hints toward using a variable convergence rate. Also, since the variable gain operation acts as a generator of higher harmonics (noises), a natural extension to the objective function would involve the addition of the variable gain output.

VIII. ACKNOWLEDGMENTS

The first author acknowledges the motivating and constructive feedback received during the review process.

REFERENCES

[1] Armstrong BSR, Gutierrez JA, Wade BA, and Joseph R. (2006) Stability of phase-based gain modulation with designer-chosen switch functions. International Journal of Robotics Research, 25(8):781-796.

[2] Eckhard D, and Bazanella AS. (2009) Optimizing the convergence of data-based controller tuning. In Proceedings of the European Control Conference, Budapest, Hungary: 910-915.

[3] Heertjes MF, Schuurbiers S, and Nijmeijer H. (2009) Performance-improved design of N-PID controlled motion systems with applications to wafer stages. IEEE Transactions on Industrial Electronics, 56(5): 1347-1355.

[4] Heertjes MF, Van Goch BPT, and Nijmeijer H. (2010) Optimal switching control of motion stages. In Proc. 5th IFAC Symposium on Mechatronic Systems, Cambridge, Massachusetts: 111-116.

[5] Huusom JK, Poulsen NK, and Jorgensen SB. (2009) Improving convergence of iterative feedback tuning. Journal of Process Control, 19(4): 570-578.

[6] Koumboulis FN, Tzamtzi MP, and Chamilothoris GE. (2007) Multivariable iterative feedback tuning - a step-wise safe switching approach. IEEE, 1354:1363.

[7] Li Y, Venkataramanan V, Guo G, and Wang Y. (2007) Dynamic nonlinear control for fast seek-settling performance in hard disk drives. IEEE Transactions on Industrial Electronics, 54(2): 951-962.

[8] Martinez JJ, Sename O, and Voda A. (2009) Modeling and robust control of Blu-ray disc servo mechanisms. Mechatronics, 19: 712-725.

[9] Meulen Van der SH, Tousain RL, and Bosgra OH. (2008) Fixed structure feedforward controller design exploiting iterative trials: application to a wafer stage and a desktop printer. Journal of Dynamic Systems, Measurement, and Control, 130(5): 051006-1/16.

[10] Stearns H, Mishra S, and Tomizuka M. (2008) Iterative tuning of feedforward controller with force ripple compensation for wafer stage. In Proceedings of the 10th IEEE International Workshop on Advanced Motion Control, Trento, Italy: 234-239.

[11] Su YX, Sun D, and Duan BY. (2005) Design of an enhanced nonlinear PID controller. Mechatronics, 15:1005-1024.